Title

Decoding allosteric regulation by the acyl carrier protein

Journal

Proceedings of the National Academy of Sciences of the United States of America, 118(16)

ISSN

0027-8424

Authors

Sztain, Terra
Bartholow, Thomas G
Lee, D John
et al.

Publication Date

2021-04-20

DOI

10.1073/pnas.2025597118

Peer reviewed

Decoding allosteric regulation by the acyl carrier protein

Terra Sztain[a], Thomas G. Bartholow[a], D. John Lee[a], Lorenzo Casalino[a], Andrew Mitchell[a], Megan A. Young[a], Jianing Wang[a], J. Andrew McCammon[a,b,1], and Michael D. Burkart[a,1]

[a]Department of Chemistry and Biochemistry, University of California San Diego, La Jolla, CA 92093-0358; and [b]Department of Pharmacology, University of California San Diego, La Jolla, CA 92093-0340

Contributed by J. Andrew McCammon, March 4, 2021 (sent for review December 12, 2020; reviewed by James Briggs and Dominique P. Frueh)

Enzymes in multistep metabolic pathways utilize an array of regulatory mechanisms to maintain a delicate homeostasis [K. Magnuson, S. Jackowski, C. O. Rock, J. E. Cronan, Jr, *Microbiol. Rev.* 57, 522–542 (1993)]. Carrier proteins in particular play an essential role in shuttling substrates between appropriate enzymes in metabolic pathways. Although hypothesized [E. Płoskoń et al., *Chem. Biol.* 17, 776–785 (2010)], allosteric regulation of substrate delivery has never before been demonstrated for any acyl carrier protein (ACP)-dependent pathway. Studying these mechanisms has remained challenging due to the transient and dynamic nature of protein–protein interactions, the vast diversity of substrates, and substrate instability [K. Finzel, D. J. Lee, M. D. Burkart, *ChemBioChem* 16, 528–547 (2015)]. Here we demonstrate a unique communication mechanism between the ACP and partner enzymes using solution NMR spectroscopy and molecular dynamics to elucidate allostery that is dependent on fatty acid chain length. We demonstrate that partner enzymes can allosterically distinguish between chain lengths via protein–protein interactions as structural features of substrate sequestration are translated from within the ACP four-helical bundle to the protein surface, without the need for stochastic chain flipping. These results illuminate details of cargo communication by the ACP that can serve as a foundation for engineering carrier protein-dependent pathways for specific, desired products.

acyl carrier protein | nuclear magnetic resonance | molecular dynamics | chain flipping

Maintaining steady-state homeostasis of complex cellular processes involves propagation of signals across interconnected networks of molecular assemblies, and the organization of enzymes within metabolic pathways offers a substantive example of such regulatory control (1). A thorough molecular understanding of these processes can benefit modifications of these pathways, particularly for bottom-up approaches to metabolic pathway engineering (2). Fatty acid biosynthesis (FAB) has served as an archetypical system for interconnected metabolic enzymes that encompasses a broad range of fundamental reactions essential for all domains of life (3). Here, a central acyl carrier protein (ACP) delivers the correct intermediate to one of multiple enzymes, not only providing substrates for the acetate pathways of primary and secondary metabolism but also serving to regulate the cell cycle and other global processes (4). Within fatty acid synthase (FAS), a series of enzymes catalyze the iterative condensation of two-carbon ketogenic units to a growing acyl chain, where each elongation is followed by stepwise reduction of the resulting β-ketone to a saturated fatty acid precursor (5). The ACP from *Escherichia coli* (AcpP) carries acyl chain lengths from 4 to 18 carbons, each of which transitions through four oxidation states, and each intermediate must be delivered to the appropriate enzyme within the 27 AcpP-binding proteins of the known interactome (6–8). How these interactions are organized cannot be easily explained by stochastic sampling of each ACP-tethered substrate by catalytic or regulatory proteins. Here we evaluate the functioning of an allosteric regulatory framework, guided by substrate identity, that regulates the protein–protein interactions required for enzyme activity within the bacterial FAS.

Traditional models of protein allostery often refer to binding of effector molecules at distal binding sites which alter active site functionality (9). Rather than containing catalytic active sites, carrier proteins function upon binding to a partner enzyme, forming a protein–protein interaction. Upon binding, substrate delivery to each enzyme within FAS requires a large conformational change by the ACP, termed "chain flipping." Here each acyl substrate, covalently tethered to a 4′-phosphopantetheine "arm" and sequestered within the ACP core, is translocated from the ACP pocket into the active site of the partner enzyme (10). Therefore, allostery described herein will refer to the classical definition which describes the phenomenon that indirect, specific protein sites are capable of modulating protein primary function (11). Here, the first site is within the ACP four-helical bundle, where cargos are sequestered, and the second site consists of the solvent exposed surface of this bundle protein, which interacts with catalytic partners.

Within FAB, many partner enzymes have active sites which perform specific chain elongation or reductive chemistries and are promiscuous to fatty acid chain length. However, some enzymes demonstrate chain length specificities that control the formation of key pathway products (*SI Appendix*, Fig. S1) (12–17). In these instances, two conflicting and still unproven hypotheses have

Significance

Acyl carrier proteins (ACPs) are involved in primary and secondary metabolic pathways, including the ubiquitous fatty acid biosynthesis, required for all domains of life. This single protein must deliver pathway intermediates to the appropriate enzyme, distinguishing between a myriad of possible intermediate-enzyme combinations. The intermediate is delivered to the active site of enzymes through a large conformational change termed "chain flipping." Whether chain flipping is a stochastic or regulated process has remained a mystery. This study provides evidence for an allosteric regulatory mechanism—demonstrating that substrates sequestered within the interior side of the four-helical ACP bundle confer structural changes to the exterior which are recognized by enzymes via protein–protein interactions—presenting a unique paradigm for understanding these biosynthetic pathways.

Author contributions: T.S., D.J.L., J.A.M., and M.D.B. designed research; T.S., T.G.B., and M.A.Y. performed research; T.S., T.G.B., D.J.L., L.C., A.M., and J.W. analyzed data; and T.S., M.A.Y., J.A.M., and M.D.B. wrote the paper.

Reviewers: J.B., University of Houston; and D.P.F., Johns Hopkins University School of Medicine.

The authors declare no competing interest.

[1]To whom correspondence may be addressed. Email: jmccammon@ucsd.edu or mburkart@ucsd.edu.

This article contains supporting information online at https://www.pnas.org/lookup/suppl/doi:10.1073/pnas.2025597118/-/DCSupplemental.

Published April 12, 2021.

been proposed concerning ACP-dependent enzyme regulation. One involves stochastic sampling, where each enzyme randomly binds ACP and samples ACP-tethered content via chain flipping into the active site (18). Another involves enzyme regulation via allosteric communication with the acyl-chain bearing ACP regulating enzyme reactivity, and ultimately controlling pathway processivity, without the need for chain flipping (18–20). Here we uncover the fundamental role of allostery in the transfer of octanoic acid from AcpP to the enzyme LipB, which re-directs the fatty acid from FAB to lipoic acid biosynthesis, demonstrating that the structural changes imparted by substrate sequestration are leveraged to control enzyme activity without the need for substrate sampling by the active site.

Characterization of ACPs bearing different chain lengths is inherently challenging to evaluate due to the lability of the 4′-phosphopantetheine thioester bond attachment of certain chain lengths. Leveraging a recently described methodology to enzymatically reverse acyl hydrolysis in situ (21), we acquired ^{1}H-^{15}N heteronuclear single quantum coherence (HSQC) NMR spectra of every physiological acyl chain length attached to AcpP. We additionally performed molecular dynamics (MD) simulations that provide a complete view of how AcpP structure is affected by sequestration of each chain length. Using solution NMR HSQC titration experiments, we discovered that the length of the acyl chain is communicated through differences in AcpP–partner protein interactions with LipB and the cognate (C8-AcpP) and noncognate (C12-AcpP) chain lengths. With selective ^{13}C labeling of the acyl chain termini, we observed that chain flipping occurs only when the specific cognate acyl chain is sequestered by AcpP. Next, we demonstrated that abrogation of this specific chain flipping could be achieved by mutation of a single surface residue discovered at the AcpP–LipB interface from MD simulations. These findings support the long-postulated hypothesis of allosteric control of ACP-dependent pathways by delineating each step in the process of acyl chain sequestration, partner-protein recognition, and chain flipping at the molecular level.

Solution NMR Elucidates Key Residues

We recently described a method that opposes hydrolysis by incorporating the acyl attachment enzyme AasS, which provided ^{1}H-^{15}N HSQC spectra of *holo*-, C4-, C8-, and C16-AcpP (21). In this study, we acquired remaining ^{1}H-^{15}N HSQC of AcpP carrying C6, C10, C12, C14, and C18 acyl chain lengths, allowing us to overlay spectra of every biological chain length of *E. coli* FAB (Fig. 1*A*). Remarkably, overlay of these spectra revealed a distinct chemical shift pattern. Though many residues of AcpP maintained a fairly similar chemical environment regardless of chain length, a few residues were significantly perturbed and followed a visible correlation between chain length and chemical shift (Fig. 1 *B* and *C*). Linear regression analysis of the chemical shifts versus chain length revealed 10 residues with R^2 values >0.9 (Datasets S1 and S2). These 10 residues, V7, S27, F28, D38, L42, E47, I54, E57, I62, and T64 (Fig. 1*D*), are highly conserved across multiple species (22), suggesting they may be critical for ACP communicating the length of the acyl chain to partner enzymes.

Isoleucine 54 shows the greatest magnitude chemical shift perturbation (CSP) between nearly every spectra, including between *holo*-AcpP and C4-AcpP, C4-AcpP and C6-AcpP, C10-AcpP and C12-AcpP, C12-AcpP and C14-AcpP, C16-AcpP and C18-AcpP, and *holo*-AcpP and C18-AcpP (Fig. 1*C* and *SI Appendix*, Fig. S2). I54 lines the bottom of the hydrophobic pocket in the loop between helices II and III. Mutations of I54 have shown it is critical for the structural integrity of AcpP (20) and binding to partner proteins (23). The CSPs between C6-AcpP and C8-AcpP, C8-AcpP and C10-AcpP, and C14-AcpP and C16-AcpP were not large in magnitude for I54, and the overall magnitude of the chemical shifts was small. This could help explain how some partner enzymes may recognize a class of medium (C6, C8, C10) or long (C14, C16) chain lengths, rather than specifically distinguishing the chain length.

Residues V7, F28, L42, I54, and I62 line the hydrophobic pocket of AcpP in crystal and NMR structures (20, 24). Residues D38, E47, and E57 make up the acidic binding face of helices II and III. This suggests a communication mechanism by which the length of the fatty acid perturbs the residues in the pocket of AcpP, leading to perturbations in residues on the surface of AcpP which directly participate in partner enzyme binding.

Molecular Dynamics Simulations Reveal Structural Signatures and Correlated Motions

To gain a better understanding of the structural implications of the observed chemical shift trends, we performed MD simulations of AcpP carrying every biological chain length of *E. coli* FAB, except for the C8 simulation which we've previously reported (25) and further analyzed here. Five independent simulations of 500 ns for each acyl chain length were carried out, all modeled from the crystal structure of heptanoyl-AcpP (Protein Data Bank [PDB] ID code 2FAD) (20). For each of the 10 key residues identified during NMR, the distance between that residue and the three main components of the ligand were monitored throughout the simulation and compared for each chain length. The main components were considered to be the phosphorus of 4′-phosphopantetheine, the linkage sulfur, or the terminal carbon of the acyl chain. For each of the AcpP residues, either one or two of the calculated distances was correlated to chain length (Fig. 2*A* and *SI Appendix*, Fig. S3). All of these distances increased with chain length, except for the distance between residues V7, I54, and E47 to the terminal carbon, which decreased with increasing chain length (*SI Appendix*, Fig. S3). This corresponded to a widening of helices II and III and loop III with increased chain length (Fig. 2*B*), and a tightening of the bottom pocket including helices I and II and loop II. Overall, an increase in the radius of gyration was observed with increasing chain length (Fig. 2*C*).

The correlated motions of each residue were quantified, revealing high correlation in all simulations of the back face of AcpP, consisting of loops I and III and helix IV (*SI Appendix*, Fig. S4). Helices II and III were anticorrelated in all simulations, indicating a possible mechanism whereby the helices open apart in opposing directions for substrate delivery and close together for substrate sequestration. This is in agreement with the mechanism observed in a steered MD study where helix III dynamics facilitated substrate delivery from ACP to FabZ (26). Reordering the correlation matrix by internal versus external residues shows a strong positive correlation between the interior pocket and exterior surface of AcpP (Fig. 2*D* and *SI Appendix*, Fig. S5). This supports an allosteric substrate communication mechanism whereby the sequestered acyl chain affects the conformation of interior helix residues which is translated to the exterior, enzyme binding interface residues (Fig. 2 *E* and *F*).

Substrate Sequestration and the 4′-Phosphopantetheine Hairpin

Expansion of the hydrophobic pocket to accommodate increasing chain lengths has been observed in crystal structures (27) and MD simulations (28). The simulations performed by Chan et al. (28) also revealed that the pocket reaches a maximum expansion volume (Fig. 2 *G* and *H*), helping to explain the increased solvent accessibility of the thioester and increased hydrolysis rates of longer chain lengths (29). However, these simulations were performed for only 20 ns each. Our 500 ns simulations showed that long chain lengths built from medium chain length structures (heptanoyl-AcpP) required up to 250 ns to fully equilibrate to the ideal substrate sequestration (*SI Appendix*, Fig. S6).

This was determined by calculating the distance between the sulfur and center of mass of AcpP. Three distinct sequestration states were observed with distances of ~5 Å (tightly sequestered),

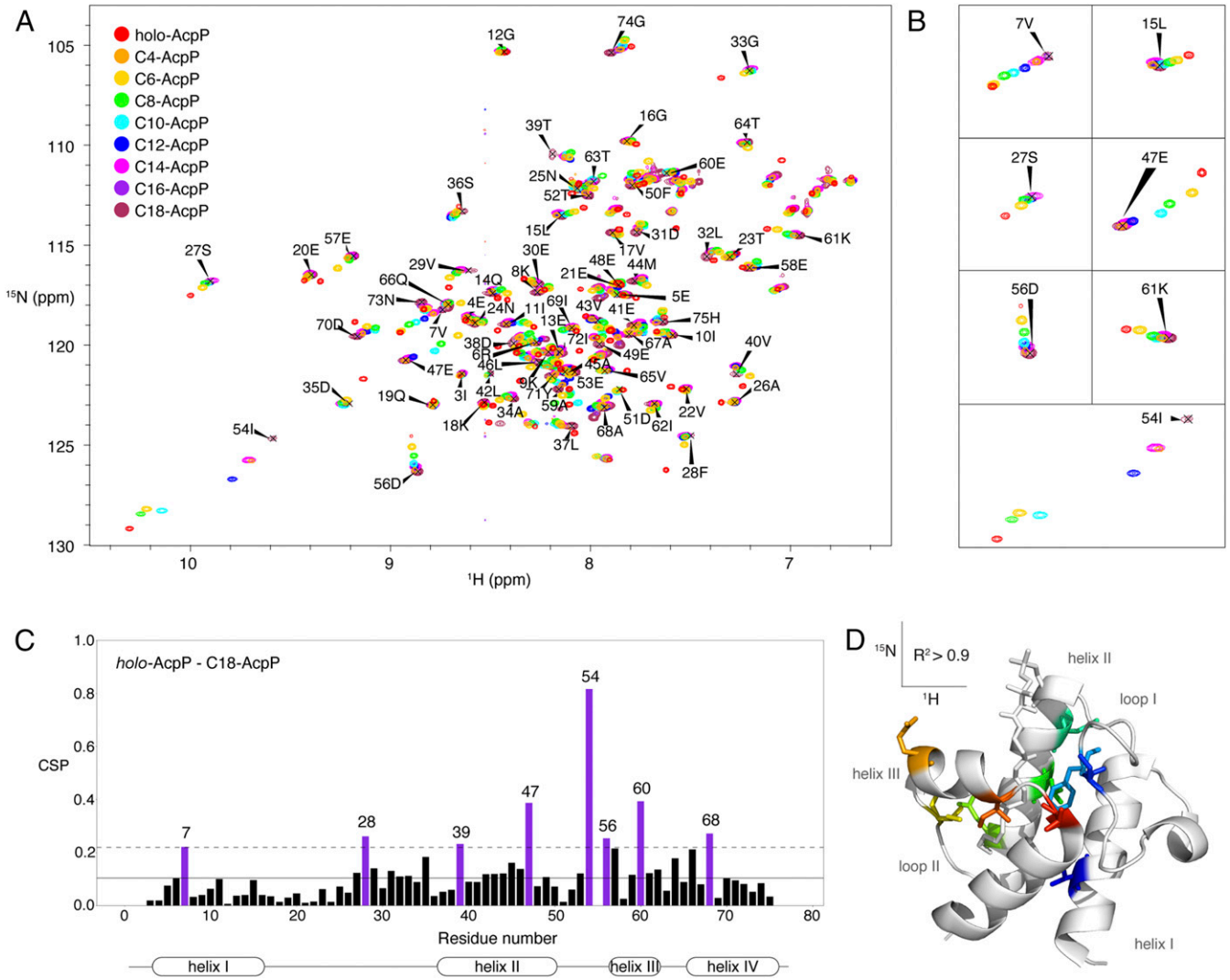

Fig. 1. Solution NMR analysis of every chain length. (*A*) ^{1}H-^{15}N HSQC NMR spectra of AcpP carrying each biological chain length fatty acid. (*B*) Selected residues demonstrating chain length-dependent chemical shift migration are enlarged, with background peaks removed for clarity. (*C*) Chemical shift perturbation plot between *holo*-AcpP and C18-AcpP with the mean shown as a solid black line and the SD shown as a dashed line. Residues above 1 SD from the mean are colored in purple. (*D*) AcpP with residues with chemical-shift perturbations correlated to chain length with R^2 value >0.9 is shown as sticks and colored in rainbow on PDB ID code 2FAD. ppm, parts per million.

6 to 8 Å (loosely sequestered), and 13 to 15 Å (unsequestered) (Fig. 2 *I* and *J*). *Holo*-AcpP was extremely dynamic and sampled all three states throughout the simulation. Short chains C4- and C6-AcpP stayed tightly sequestered, while medium chains C8- and C10-AcpP spent some time in the tightly sequestered state, though they spent the majority of the simulation in the loosely sequestered state. C12-AcpP spent even less time tightly sequestered, most time loosely sequestered, and sampled the unsequestered state. Long chains C14-, C16-, and C18-AcpP spent the majority of the simulation in the loosely sequestered state and also sampled the unsequestered state. Histogram peaks corresponding to tight sequestration disappeared for C14-, C16-, and C18-AcpP when the beginning of the trajectories was not included in the calculation but did not decrease for C12-AcpP. Complete loss of these peaks required 250 ns (*SI Appendix*, Fig. S6). Zornetzer et al. (29) previously reported NMR experiments showing that chain length can affect dynamics of spinach ACP.

Trajectories representing principal component analysis of each simulation revealed structural and dynamic properties of the motion underlying the speculated "hairpin" formation of 4′-phosphopantetheine and corresponded to the distance between the sulfur and center of mass in many simulations (*SI Appendix*, Figs. S7 and S8 and Movie S1). The key residue F28 appears to facilitate the hairpin formation, acting as a ruler by which only around eight carbons can fit securely in the hydrophobic pocket (Fig. 2*K*). The acyl chain was observed sliding in and out of the hydrophobic pocket, equilibrating to, and then remaining dynamic within one of the three sequestration states in each of the trajectories.

AcpP Communicates Substrate Identity through Protein–Protein Interactions

In order to determine how AcpP uses these key residues during protein–protein interactions with a partner enzyme, we performed NMR titration experiments with the chain length-specific enzyme LipB. This enzyme selectively harnesses C8-AcpP from FAB for the biosynthesis of lipoic acid. We increased molar equivalents of inactive LipB (C169A active site mutation to prevent hydrolysis or covalent attachment) (30) with ^{15}N-labeled C8-AcpP or C12-AcpP and acquired ^{1}H-^{15}N HSQC spectra at each titration point up to 1.5 equivalents of LipB (Fig. 3 *A*–*D*). Though a few

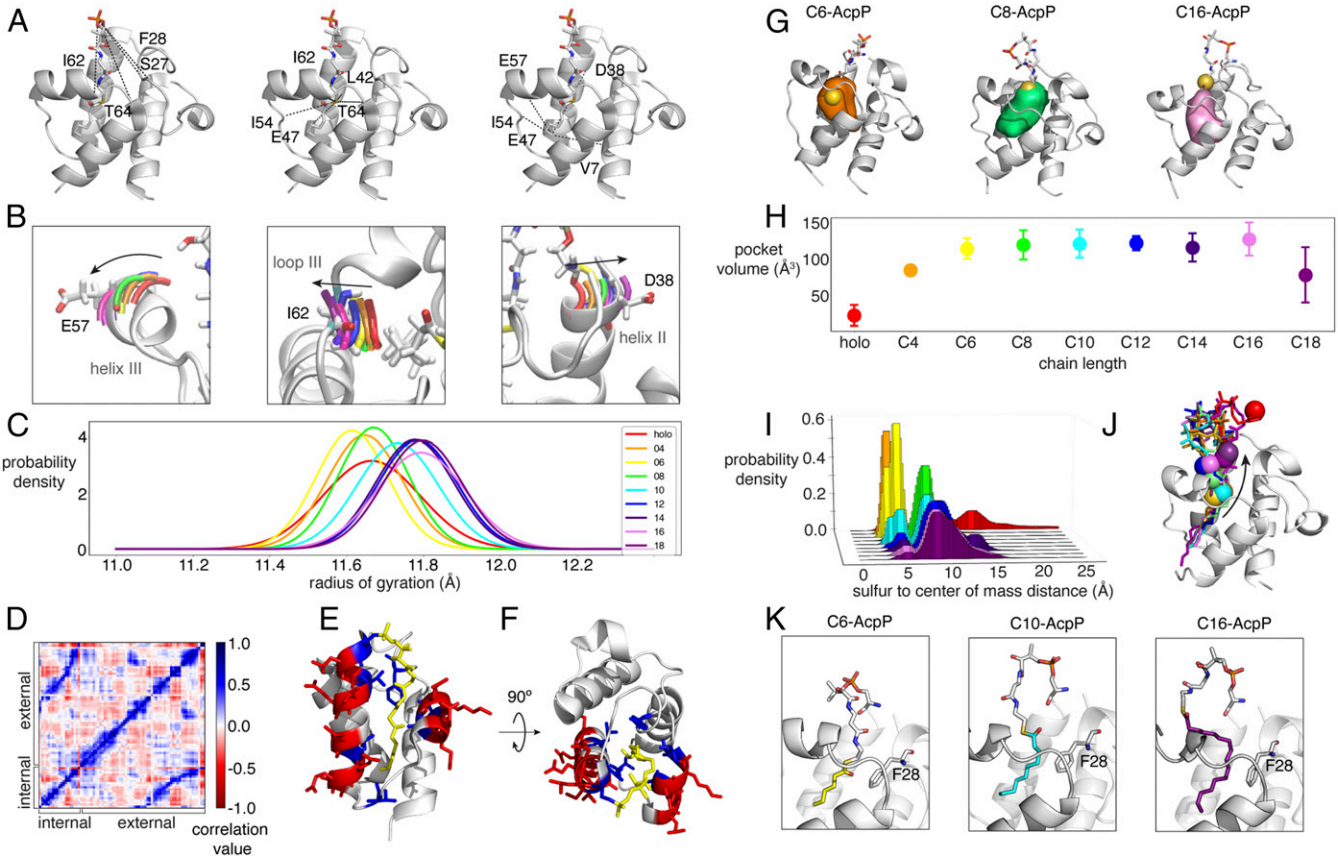

Fig. 2. MD analysis of acyl chain length on the AcpP structure. (*A*) Distances which are correlated with chain length with R^2 >0.6 of residue to phosphorus, sulfur, or the terminal carbon shown on PDB ID code 2FAD. (*B*) Backbone residues shown in tube representation with increasing chain lengths colored and shown with black arrows. (*C*) Normalized probability density of the radius of gyration calculated from the total 2.5 μs simulated of each chain length. (*D*) Correlated motion map reordered to show correlations between internal and external residues. (*E*) AcpP from PDB ID code 2FAD with the acyl chain colored in yellow, internal residues colored in blue, and select external residues colored in red. (*F*) Top-down view of *E*. (*G*) Representative structures of C6-, C8-, and C16-AcpP with the pocket shown in orange, green, and pink, respectively. The sulfur atom is shown as a gold sphere. (*H*) Calculated pocket volume for each chain length. Error bars represent deviation from the mean from five independent simulations. (*I*) Histograms of the distance from the sulfur atom to the center of mass of acyl-AcpP calculated from the total 2.5 μs simulation of each acyl-AcpP. (*J*) Structure representing the distance calculated in *I* with sulfur shown as a gold sphere. The black arrow indicates the direction of the sulfur atom as the distance to center of mass is increased with increased chain length. (*K*) Representative structures of C6-, C10-, and C16-AcpP from MD simulations with acyl chains shown relative to residue F28.

peaks were lost due to signal dampening in the presence of LipB, a clear difference in AcpP perturbation by LipB was observed depending on chain length. The cognate, C8-AcpP was perturbed at helices II and III, whereas the noncognate C12-AcpP was only perturbed at helix II, and the magnitude of perturbations was greater than that of C8-AcpP (Fig. 3 *E*, *F*, and *H*). Lineshape analysis was carried out using TITAN software (31) to determine the K_d and k_{off} from the titration data, showing larger values for each of C12-AcpP compared with C8-AcpP. This demonstrates both a kinetic and thermodynamic favoring toward binding to AcpP when the specific substrate is bound. The key residue, E57, was perturbed greater than 1 SD from the mean by LipB for C8-AcpP but not C12-AcpP. The more open position and outward rotation formed by C12-AcpP compared with C8-AcpP observed in MD simulations (Fig. 2*C*) are likely not as suitable of a binding interface for LipB. This was supported by docking a homology model of *E. coli* LipB derived from *Thermus thermophilus* LipB PDB ID code 2QHS (32) (*SI Appendix*, Fig. S9) to MD-derived C8-AcpP and C12-AcpP structures, where hydrogen bonds were observed between R145 of LipB and E57 in C8-AcpP but not in the C12-AcpP structure. In the C12-AcpP structure, helix III is shifted to accommodate the longer acyl chain through interaction of I54 (Fig. 1 *A* and *B*), disallowing E57 from forming a salt bridge with R145 (Fig. 3*G*).

Substrate-Specific Chain Flipping

To determine whether these differences in protein–protein interactions play a significant role in communicating chain length identity, we sought to determine whether chain flipping could still occur with a noncognate acyl chain length. Previous efforts to visualize chain flipping have involved attachment of nonphysiological cargo, such as fluorescent or solvatochromic adducts (33). Here we designed an NMR experiment to detect chain flipping of a native acyl-AcpP (Fig. 4*A*). We obtained ^{13}C-labeled octanoic and dodecanoic acids selectively labeled at the terminal carbon (ω-1-^{13}C). Acquisition of ^{1}H-^{13}C HSQC NMR spectra of the fatty acids alone in solution gave peaks with distinct chemical shifts compared with those when covalently attached to AcpP (*SI Appendix*, Fig. S11). Addition of 1.5 equivalents of LipB (C169A) resulted in emergence of a second peak, apparently undergoing a slow exchange, with only C8-AcpP (Fig. 4 *B* and *C*) and not C12-AcpP (Fig. 4 *E* and *F*). The new peak, significantly downfield from the free or AcpP-sequestered peak, indicates a much less shielded environment upon chain flipping into the LipB pocket. Several smaller peaks are present in this spectrum, which we

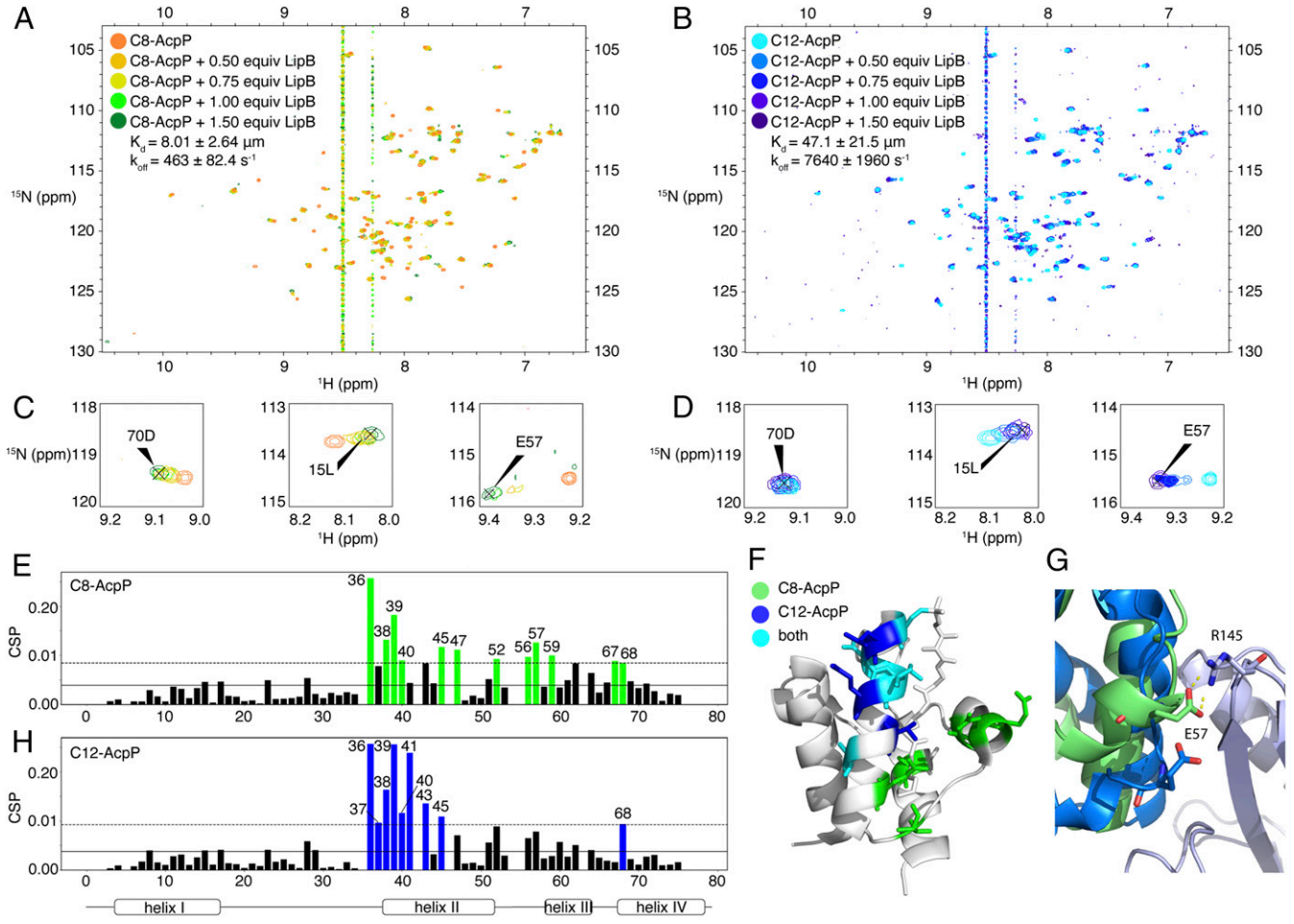

Fig. 3. Protein–protein interaction analysis of cognate and noncognate chain lengths via NMR titration and docking. (*A*) ^{1}H-^{15}N HSQC spectrum overlay of C8-AcpP titrated with increasing equivalents of LipB. (*B*) ^{1}H-^{15}N HSQC spectrum overlay of C12-AcpP titrated with increasing equivalents of LipB. The interfering signals around 8.3 and 8.5 ppm are a result of t_1 noise due to the presence of adenosine triphosphate at high concentration within the buffer components (*SI Appendix*, Fig. S10), which was used for consistency with Fig. 1 as detailed in *SI Appendix, NMR Methods*. (*C* and *D*) Enlarged view of selected peaks from *A* and *B*, respectively. (*E* and *H*) CSP plots quantifying *A* and *B*, respectively. The solid line represents the mean, and the dashed line represents 1 SD from the mean. Residues with CSP values above 1 SD from the mean are colored in green or blue. (*F*) CSP residues colored on PDB ID code 2FAD based on whether they are above 1 SD from the mean in C8-AcpP titration only (green), C12-AcpP titration only (blue), or both (cyan). (*G*) Docking interface of LipB (purple) to C8-AcpP (green) and C12-AcpP (blue).

hypothesize may be metastable intermediates that make up less than 10% of the intensity of the upfield peak and were not included in quantifying the percentage of sequestered and flipped peak intensity.

To confirm the identity of the chain-flipped peak, we compared the spectra of both ω-1-^{13}C–labeled free fatty acids (C8 and C12) in the presence of only LipB. In the case of octanoic acid with LipB, there were no peaks resembling the free fatty acid, only the intense peak in the same location as the chain-flipped peak from the C8-AcpP study, along with similar minor downfield peaks (*SI Appendix*, Fig. S11*A*), indicative of binding to the hydrophobic pocket of the LipB active site. The spectrum of dodecanoic acid, however, showed little change upon addition of LipB (*SI Appendix*, Fig. S12*B*). Binding of free octanoic acid within the LipB active site has been observed by X-ray crystallography following crystal soaking experiments of the *T. thermophilus* LipB with octanoic acid (32), confirming our assignment of fatty acid binding within the LipB active site. We therefore confidently assigned this downfield peak as "flipped" compared to the AcpP "sequestered."

The chain flipping detection experiment indicated that chain flipping is indeed avoided by the chain length-specific partner enzyme LipB when AcpP bears a noncanonical acyl chain length. The nature of this specific chain flipping is apparently due to the differences in protein–protein interactions of LipB with AcpP depending on whether AcpP carries the correct acyl chain length. To test this, we designed an interface mutant guided by the NMR and MD characterization of AcpP structure with each acyl chain length.

The residue E57 was one of the 10 key residues found to be important for chain length communication by NMR (Fig. 1*D*) and MD (Fig. 2 *C* and *D*). Residue E57 was also perturbed by LipB, with CSP greater than 1 SD from the mean, in C8-AcpP but not C12-AcpP (Fig. 3 *E* and *H*), and participated in hydrogen bonding with R145 when docked to LipB in the C8-AcpP but not C12-AcpP structure (Fig. 3*G*). Therefore, we generated an R145A mutant of LipB and evaluated chain flipping with selective ^{13}C-labeled C8-AcpP and C12-AcpP. This experiment identified chain flipping of both C8-AcpP and C12-AcpP species (Fig. 4 *D* and *G*), indicating the acyl chain length specificity was disrupted by eliminating this interfacial interaction. We suspect that LipB R145 behaves as a gating residue that is opened upon salt bridge formation with AcpP E57 only when the proper binding orientation is formed, which occurs with C8-AcpP but not C12-AcpP. In this case, elimination of the gate leads to a more promiscuous LipB, which also induces chain flipping from C12-tethered AcpP.

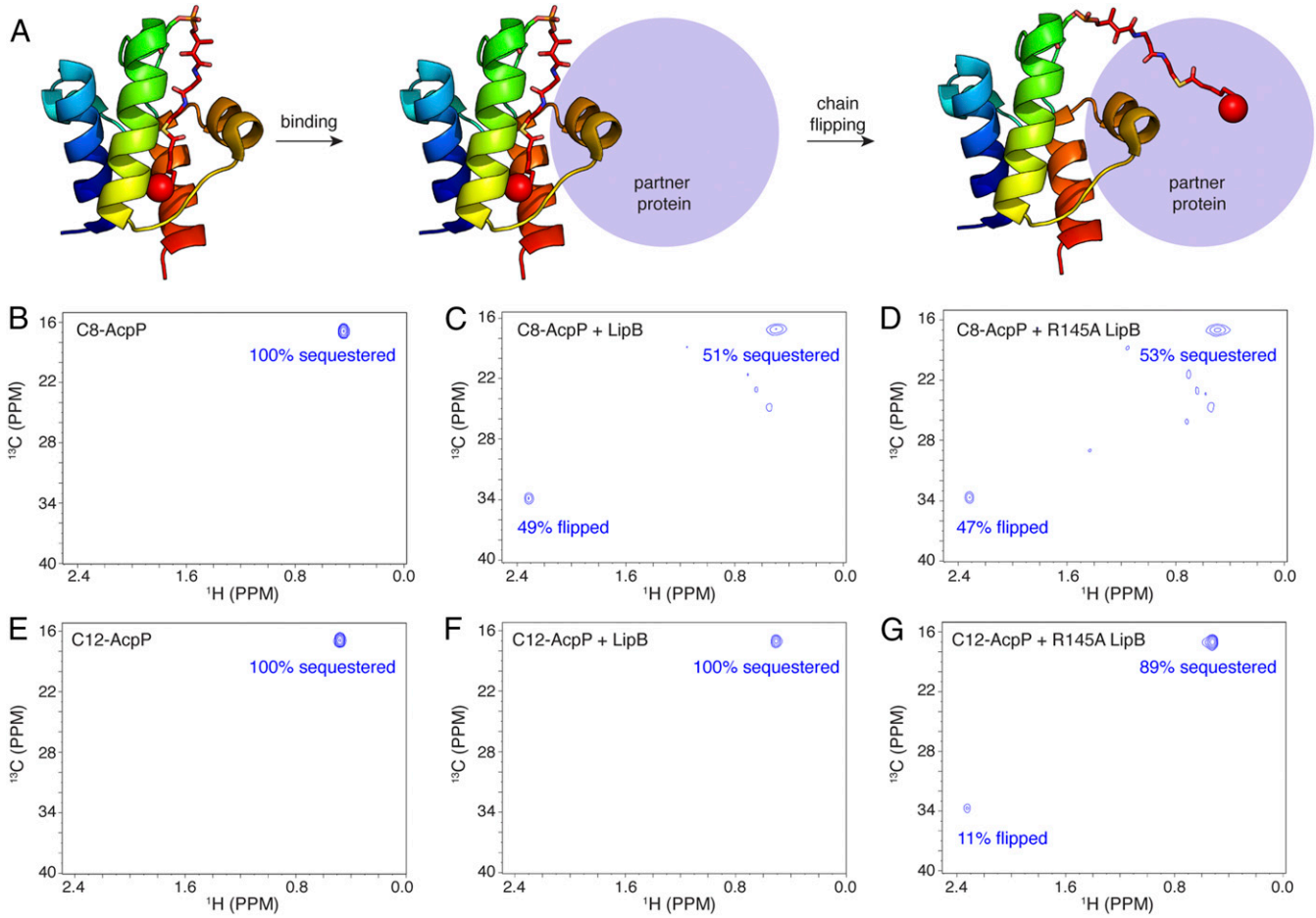

Fig. 4. Chain flipping of cognate and noncognate chain lengths. (*A*) Schematic of chain flipping, with the terminal carbon which was selectively ^{13}C-labeled in the following experiments shown as a red sphere. (*B–D*) ^{1}H-^{13}C HSQC NMR spectra of C8-AcpP with the terminal C8 ^{13}C-labeled. The relative intensities of each peak are labeled as a percentage if they are >10% intensity compared with the sequestered peak. Spectra were acquired with C8-AcpP alone (*B*), in the presence of 1.5 equivalents of C169A LipB (*C*), and in the presence of 1.5 equivalents of R145A C169A LipB mutant (*D*). (*E–G*) ^{1}H-^{13}C HSQC NMR spectra of C12-AcpP with the terminal C12 ^{13}C-labeled. Spectra were acquired with C12-AcpP alone (*E*), in the presence of 1.5 equivalents of C169A LipB (*F*), and in the presence of 1.5 equivalents of R145A C179A LipB mutant (*G*).

Conclusion

Metabolic pathways in nature rely on an intricately choreographed series of reactions carried out by many enzymes. Advances in structural techniques can enable detailed accounts of the regulatory mechanisms governing these pathways. One central metabolic protein that has eluded full understanding is the ACP from fatty acid biosynthesis. This small, 77-residue protein interacts with dozens of enzymes and regulatory proteins, delivering each the appropriate acyl chain length and oxidation state substrate. The role of ACP as an active controller or passive carrier (18), and whether the universal chain flipping mechanism (10) is a stochastic event required for substrate recognition or triggered by a specific binding event, has been under discussion for decades. These results demonstrate that a specific pattern of structural changes in ACP can communicate the length of the acyl chain to a partner enzyme via protein–protein interactions, thereby allosterically regulating the chain flipping event. These findings represent a unique paradigm for understanding multistep, carrier protein-dependent biosynthetic pathways. The highly detailed evaluation of AcpP bearing each fatty acid chain length provided here will serve as a foundation for gaining more detailed control for engineering specific acyl chain length products or designing narrow-spectrum antibiotics targeting specific protein–protein interactions.

Data Availability. Molecular dynamics structure data reported in this article have been deposited in GitHub (https://github.com/tsztain/AcpP_MD).

ACKNOWLEDGMENTS. We thank Prof. Stanley Opella and Prof. Lalit Deshmukh for helpful NMR discussions. We are also grateful for Dr. Xuemei Huang's assistance with NMR acquisition. T.S. is an NSF Graduate Research Fellowship Program recipient under Grant DGE-1650112. This work was supported by NIH GM031749 and GM095970.

1. M. Whiteley, S. P. Diggle, E. P. Greenberg, Progress in and promise of bacterial quorum sensing research. *Nature* **551**, 313–320 (2017).
2. J. Beld, D. J. Lee, M. D. Burkart, Fatty acid biosynthesis revisited: Structure elucidation and metabolic engineering. *Mol. Biosyst.* **11**, 38–59 (2015).
3. C. O. Rock, S. Jackowski, Forty years of bacterial fatty acid synthesis. *Biochem. Biophys. Res. Commun.* **292**, 1155–1166 (2002).
4. K. Magnuson, S. Jackowski, C. O. Rock, J. E. Cronan, Jr, Regulation of fatty acid biosynthesis in *Escherichia coli*. *Microbiol. Rev.* **57**, 522–542 (1993).
5. D. A. Hopwood, D. H. Sherman, Molecular genetics of polyketides and its comparison to fatty acid biosynthesis. *Annu. Rev. Genet.* **24**, 37–66 (1990).
6. C. Nguyen *et al*., Trapping the dynamic acyl carrier protein in fatty acid biosynthesis. *Nature* **505**, 427–431 (2014).
7. N. R. De Lay, J. E. Cronan, In vivo functional analyses of the type II acyl carrier proteins of fatty acid biosynthesis. *J. Biol. Chem.* **282**, 20319–20328 (2007).
8. D. Gully, E. Bouveret, A protein network for phospholipid synthesis uncovered by a variant of the tandem affinity purification method in *Escherichia coli*. *Proteomics* **6**, 282–293 (2006).

9. R. Nussinov, C.-J. Tsai, B. Ma, The underappreciated role of allostery in the cellular network. *Annu. Rev. Biophys.* **42**, 169–189 (2013).
10. J. E. Cronan, The chain-flipping mechanism of ACP (acyl carrier protein)-dependent enzymes appears universal. *Biochem. J.* **460**, 157–163 (2014).
11. J. Monod, J. Wyman, J.-P. Changeux, On the nature of allosteric transitions: A plausible model. *J. Mol. Biol.* **12**, 88–118 (1965).
12. S. W. Jordan, J. E. Cronan, Jr, The *Escherichia* coli lipB gene encodes lipoyl (octanoyl)-acyl carrier protein:protein transferase. *J. Bacteriol.* **185**, 1582–1589 (2003).
13. C. R. H. Raetz *et al*., Discovery of new biosynthetic pathways: The lipid A story. *J. Lipid Res.* **50** (suppl.), S103–S108 (2009).
14. J. P. Issartel, V. Koronakis, C. Hughes, Activation of *Escherichia coli* prohaemolysin to the mature toxin by acyl carrier protein-dependent fatty acylation. *Nature* **351**, 759–761 (1991).
15. M. J. Grisewood *et al*., Computational redesign of acyl-ACP thioesterase with improved selectivity toward medium-chain-length fatty acids. *ACS Catal.* **7**, 3837–3849 (2017).
16. Y.-M. Zhang, C. O. Rock, Thematic review series: Glycerolipids. Acyltransferases in bacterial glycerophospholipid synthesis. *J. Lipid Res.* **49**, 1867–1874 (2008).
17. R. J. Heath, C. O. Rock, Roles of the FabA and FabZ β-hydroxyacyl-acyl carrier protein dehydratases in *Escherichia coli* fatty acid biosynthesis. *J. Biol. Chem.* **271**, 27795–27801 (1996).
18. J. Crosby, M. P. Crump, The structural role of the carrier protein—Active controller or passive carrier. *Nat. Prod. Rep.* **29**, 1111–1137 (2012).
19. E. Płoskoń *et al*., Recognition of intermediate functionality by acyl carrier protein over a complete cycle of fatty acid biosynthesis. *Chem. Biol.* **17**, 776–785 (2010).
20. A. Roujeinikova *et al*., Structural studies of fatty acyl-(acyl carrier protein) thioesters reveal a hydrophobic binding cavity that can expand to fit longer substrates. *J. Mol. Biol.* **365**, 135–145 (2007).
21. T. Sztain, T. G. Bartholow, J. A. McCammon, M. D. Burkart, Shifting the hydrolysis equilibrium of substrate loaded acyl carrier proteins. *Biochemistry* **58**, 3557–3560 (2019).
22. D. M. Byers, H. Gong, Acyl carrier protein: Structure-function relationships in a conserved multifunctional protein family. *Biochem. Cell Biol.* **85**, 649–662 (2007).
23. S. Angelini, L. My, E. Bouveret, Disrupting the acyl carrier protein/SpoT interaction in vivo: Identification of ACP residues involved in the interaction and consequence on growth. *PLoS One* **7**, e36111 (2012).
24. B.-N. Wu, Y.-M. Zhang, C. O. Rock, J. J. Zheng, Structural modification of acyl carrier protein by butyryl group. *Protein Sci.* **18**, 240–246 (2009).
25. T. Sztain *et al*., Modifying the thioester linkage affects the structure of the acyl carrier protein. *Angew. Chem. Int. Ed. Engl.* **58**, 10888–10892 (2019).
26. F. Colizzi, M. Masetti, M. Recanatini, A. Cavalli, Atomic-level characterization of the chain-flipping mechanism in fatty-acids biosynthesis. *J. Phys. Chem. Lett.* **7**, 2899–2904 (2016).
27. A. Roujeinikova *et al*., Crystallization and preliminary X-ray crystallographic studies on acyl-(acyl carrier protein) from *Escherichia coli*. *Acta Crystallogr. D Biol. Crystallogr.* **58**, 330–332 (2002).
28. D. I. Chan, T. Stockner, D. P. Tieleman, H. J. Vogel, Molecular dynamics simulations of the apo-, holo-, and acyl-forms of *Escherichia coli* acyl carrier protein. *J. Biol. Chem.* **283**, 33620–33629 (2008).
29. G. A. Zornetzer, J. Tanem, B. G. Fox, J. L. Markley, The length of the bound fatty acid influences the dynamics of the acyl carrier protein and the stability of the thioester bond. *Biochemistry* **49**, 470–477 (2010).
30. X. Zhao, J. R. Miller, J. E. Cronan, The reaction of LipB, the octanoyl-[acyl carrier protein]:protein *N*-octanoyltransferase of lipoic acid synthesis, proceeds through an acyl-enzyme intermediate. *Biochemistry* **44**, 16737–16746 (2005).
31. C. A. Waudby, A. Ramos, L. D. Cabrita, J. Christodoulou, Two-dimensional NMR lineshape analysis. *Sci. Rep.* **6**, 24826 (2016).
32. D. J. Kim *et al*., Structural basis of octanoic acid recognition by lipoate-protein ligase B. *Proteins* **70**, 1620–1625 (2008).
33. J. Beld, H. Cang, M. D. Burkart, Visualizing the chain-flipping mechanism in fatty-acid biosynthesis. *Angew. Chem. Int. Ed. Engl.* **53**, 14456–14461 (2014).